Production and Magnetic Properties of Co- and La–Y-Doped Strontium Ferrite

B. Ertug*

Bilgi University, Faculty of Engineering and Natural Sciences, Eski Silahtarağa Elektrik Santralı Kazım Karabekir Cad. No: 2/13, 34060 Istanbul, Turkey

Received: 20.06.2024 & Accepted: 29.07.2024

Doi: 10.12693/APhysPolA.146.279 *e-mail: burcuertug@gmail.com

In this study, rare earth-substituted M-type Sr-hexaferrites with the chemical compositions $Sr_{1-x}(RE)_xFe_{12-x}Co_xO_{19}$ and $Sr_{1-2x}(RE)_{2x}Fe_{12-x}Co_xO_{19}$ were prepared using the solid-state reaction method. All of the hexaferrite samples were characterized using instrumental techniques of X-ray diffraction, optical microscopy, and vibrating sample magnetometer to study the effect of La–Y substitution on the structural and magnetic properties. The bulk densities changed from 4.45 to 4.96 g/cm^3 after sintering at 1250°C. X-ray diffraction diagrams of all the sintered samples confirmed that the Sr-hexaferrite phase persisted with La/Y and Co co-substitution without secondary phases. However, the substitution affected the peak intensities and the positions of Bragg angles. The reduction in the saturation magnetization (M_s) was observed from 25.4 emu/g for single La to 9.40 emu/g for La–Y substitution. It was found that the coercivity (H_c) improved from 502 to 2080 Oe for a single Y-substituted sample and a single La-substituted sample, respectively. The measured squareness ratio (M_r/M_s) was larger than 0.5, indicating that the change in the magnetization can be realized by the rotation. The results suggest that the incorporation of rare-earth cations can improve the magnetic properties of strontium hexaferrites.

topics: strontium hexaferrite, ferrimagnetic, doping, rare earth

1. Introduction

Magnetic hyperthermia is a type of cancer treatment during which magnetic nanoparticles or thermoseeds generate the heating under the magnetic field to destroy the malignant cells. In 2023, Radon and co-workers [1] explored magnetically induced hyperthermia and conducted a biocompatibility study. The biomaterials having high saturation magnetization provide an efficient therapeutic treatment against these malignant cells. The maghemite (γ-Fe_2O_3) and magnetite (Fe_3O_4), as the ferromagnetic phases, are the candidate biomaterials that are considered for use in this magnetic hyperthermia technique [2]. The surface of the magnetite nanoparticles is modified to produce biocompatible nanoplatforms against cancer [3–5].

During the application of magnetic hyperthermia, the local temperature rise (42–46°C) is provided under the magnetic field, destroying the cancer tissue. Protein scaffolding is weakened through this temperature rise inside the nucleus of the cancer cell, and then the nuclear DNA becomes vulnerable towards radiation and chemotherapy [6].

Strontium hexaferrites have aroused considerable interest in the research field of magnetic properties. In addition, this material is beneficial as a permanent magnet due to high magnetocrystalline anisotropy having a single magnetization axis, high saturation magnetization, high Curie temperature, as well as corrosion resistance and excellent chemical stability [7, 8].

Hexaferrite materials are widely used for a number of applications such as magnetic recording and the absorption of electromagnetic radiation in the microwave range [9, 10]. Other important applications of hexaferrite materials are computer data storage, magneto-optic recording, and magnetic fluids [11]. The specific magnetic properties of the Sr-hexaferrites arise due to the interaction between the metallic ions in the hexagonal crystal lattice and the oxygen anions [12].

The traditional method of producing strontium hexaferrites is known as the solid-state reaction. Steier and colleagues [13] explained the formation of hexaferrites according to the solid-state reaction. This method consists of two stages, namely

$$SrCO_3 + Fe_2O_3 \rightarrow SrFe_2O_4 + CO_2, \quad (1)$$

$$SrFe_2O_4 + 5Fe_2O_3 \rightarrow SrO \cdot 6Fe_2O_3. \quad (2)$$

The decarboxylation occurs, which is accompanied by the formation of $SrFe_2O_4$ monoferrite, see (1). Afterwards, the cation of Sr^{2+} diffuses into the iron (3+) oxide. In this method, the starting powders are

Fig. 1. Samples of Co- and La–Y-doped Sr-ferrite.

TABLE I

Relative density and porosity results.

Label	Theoretical density [g/cm^3]	Relative density [%]	Porosity P [%]
SFL	5.11	95	5
SFY	5.11	87	13
SFLY2	5.11	88	12
SFLY1	5.11	97	7

mixed and then sintered at around 1000°C, and the resultant particles have a size of ≈ 1 μm [14]. Some other production techniques, such as controlled crystallization, chemical coprecipitation, sol–gel, and self-propagation high-temperature synthesis, are also utilized to obtain finer particle sizes. Because of the high cost and complexity of these methods, we preferred to use the traditional solid-state reaction for the Sr-hexaferrites [15].

An efficient approach to modify the magnetic properties of the M-type hexaferrites is the substitution by various cations. In an earlier study, the substitution by Co–Mg was reported to produce a co-doped Sr-hexaferrite [16]. The substitution of Fe^{3+} by a trivalent cation, Co^{3+}, was also reported to produce and characterize a nanocomposite [17]. On the other hand, some attention has been given to the magnetic results of the substitution of Ba or Sr by the rare-earth elements. Various examples of these studies include La–Co [18], Cu–Gd [19], and La–Cu [20] substitutions to the M-type strontium hexaferrite. These studies cover a co-substitution with a transition metal along with a rare-earth element. In this work we aimed to investigate the effects of a transition metal (here — Co) together with two kinds of rare-earth elements (here — La–Y) on the magnetic properties of strontium hexaferrite.

2. Experimental methods

Four hexaferrite samples with different doping percentages were synthesized and labelled as SFL, SFY, SFLY1, and SFLY2. The correspondence of the label to a given compound is as follows: SFL — $Sr_{1-x}(La)_xFe_{12-x}Co_xO_{19}$ ($x = 0.2$); SFY — $Sr_{1-x}(Y)_xFe_{12-x}Co_xO_{19}$ ($x = 0.2$); SFLY2 — $Sr_{1-2x}(La,Y)_xFe_{12-x}Co_xO_{19}$ ($x = 0.2$); and SFLY1 — $Sr_{1-2x}(La,Y)_xFe_{12-x}Co_xO_{19}$ ($x = 0.1$). The starting materials for the present synthesis include strontium carbonate ($SrCO_3$) and hematite (Fe_2O_3) powder as the main ingredients. La_2O_3 and Y_2O_3 powders were utilized for co-doping the hexaferrite.

Additionally, Co_2O_3 (99 wt % purity, particle size 44 μm, Nanokar) was used to replace Fe^{3+}. Stearic acid was used as an agent for process control. The solid-state reaction process started with mixing the powder in an agate mortar. Then, powder mixtures were placed in a hydraulic pressing machine to obtain Sr-hexaferrite samples. They were then compressed to reach near-full densification. Finally, the pellets were sintered at 1250°C for 3 h in an oxide furnace to ensure the formation of the $SrFe_{12}O_{19}$ compound, as shown in Fig. 1. Afterwards, the furnace was cooled to room temperature at a moderate rate.

The powder mixtures were identified by X-ray diffraction (XRD) in the 2θ range of 20–70° using Cu K_α radiation ($\lambda = 0.15405$ nm). X-ray diffractometer used was Rigaku D/Max-2100. The microstructural images were taken with an optical microscope at different magnifications.

The relative densities were determined through the porosity, based on the bottle pycnometer method, using water as the liquid medium, i.e.,

$$P = \frac{(w2-w1)}{(w2-w1)-(w3-w4)}, \tag{3}$$

where P is porosity; w_1 is mass of empty volume of pycnometer; w_2 — mass of pycnometer and sample; w_3 — mass of pycnometer, sample, and water; w_4 — mass of pycnometer full of water in grams [21]. The relative densities were calculated considering the theoretical density of 5.1 g/cm^3 for Sr-hexaferrite.

The ferrimagnetic properties of the co-doped hexaferrites were measured with a vibrating sample magnetometer (VSM) using Dexing Magnet VSM-550 at room temperature at a magnetic field of up to 10 kOe. The magnetic parameters were determined using the M–H hysteresis loops.

3. Results and discussion

Table I represents the relative density and the porosity results. The bulk densities changed from 4.45 to 4.96 g/cm^3 after sintering at 1250°C. These values were consistent with the density values (4.7–5.0 g/cm^3) given in a recent study, where Sr-hexaferrite was substituted with La–Co and sintered at a similar temperature (1230°C) [18].

The main phase and purity of the samples sintered at 1250°C for 3 h were determined from the XRD patterns shown in Fig. 2. All of the diffraction peaks were indexed as hexagonal strontium

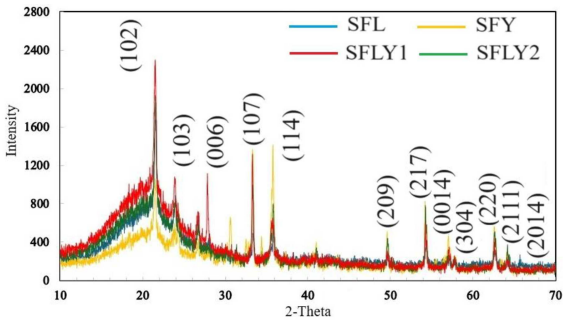

Fig. 2. XRD patterns of the obtained hexaferrites.

hexaferrite. Also, no characteristic peak belonging to an impurity oxide phase was detected. This showed that the formation of the $SrFe_{12}O_{19}$ compound was accomplished completely under the sintering conditions. Similar to our XRD results, Co–Mg co-doped Sr-hexaferrites were indexed to the magnetoplumbite structure in a previous study [16]. Also, another study on the Sr-hexaferrite/Co nanocomposites confirmed our XRD results, and the formation of the impurities was avoided in that study [17]. On the other hand, research on the Si substitution of strontium hexaferrite showed the formation of a secondary Fe_2O_3 phase [18]. The effect of Co and binary La–Y doping on the XRD patterns of the synthesized Sr-hexaferrite samples can also be seen in Fig. 2, which shows that there were some differences between the samples in terms of peak intensities and the positions of Bragg angles.

The optical microscopy images are given in Figs. 3 and 4. As observed from the images, homogeneous morphology was present in the microstructure of the samples. As confirmed with the relative density (i.e., 97 %) results, porosity was not observed in the optical images. Similar to our study, You and co-workers [18] in 2022 utilized the conventional ceramic process to obtain average low porosity values in the range of 0.1–8% [18]. After the sintering step at 1250°C for 3 h, no change was observed in the morphologies of the SFY, SFLY1, and SFLY2 samples, except that the microstructure of the SFL sample appeared to be different, showing a higher interconnected structure.

Hexagonal strontium hexaferrite was the major phase in all of the samples studied here. In addition, a greater degree of crystallization process of $SrFe_{12}O_{19}$ was observed for all XRD patterns, and this result relies on the sintering temperature. The crystal is known to be a growth process around a nucleus.

Hence, the crystal size predicted from the optical microscopy images was a function of sintering temperature, which can be controlled or altered by adjusting the annealing temperature [8]. The sintering process can significantly improve the ferrimagnetic parameters of strontium hexaferrites. Wang and colleagues [7] reported that the sintering

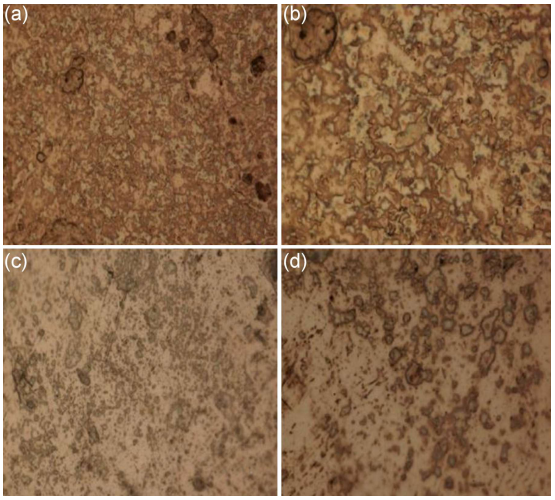

Fig. 3. Optical images of (a, b) SFL, (c, d) SFY. Magnification: (a, c) 500× and (b, d) 1000×.

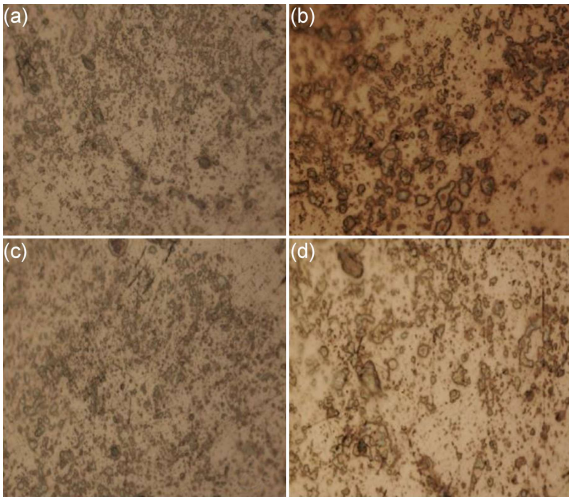

Fig. 4. Optical images of (a, b) SFLY2, (c, d) SFLY1. Magnification: (a, c) 500× and (b, d) 1000×.

process in air atmosphere can decrease the concentration of oxygen vacancies, which can change the amount of near neighbour oxygens and iron. As a result, this effect can contribute more to the superexchange interaction of Fe–O–Fe, and the ferrimagnetic properties of Sr-hexaferrite are improved [7].

Figure 5 shows the magnetic hysteresis curves for the Sr-hexaferrite samples measured at room temperature. For the M–H loops, the interrelated magnetic parameters (the saturation and remanence magnetizations and the coercivity) are listed in Table II.

The hysteresis loop of the Sr-hexaferrite sample of SFL exhibited the highest saturation magnetization, M_s = 25.4 emu/g, and the coercivity value, H_c = 2.08 kOe. According to a very recent study, La-substituted hexaferrite had M_s

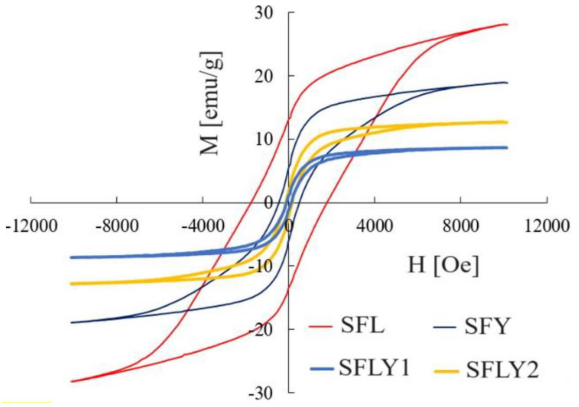

Fig. 5. Hysteresis loops of SFL, SFY, SFLY1, and SFLY2.

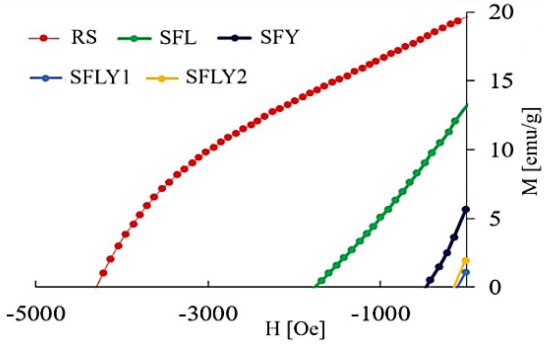

Fig. 6. Max. energy product $(BH)_{\max}$ of SFL, SFY, SFLY1, and SFLY2.

value of 22.17 emu/g, and its coercivity value was 3.338 kOe. These values are consistent with the results of our study [20]. The value of the saturation magnetization M_s of Sr-hexaferrite reference material was 33.6 emu/g, its max. energy product was $(BH)_{\max} = 148.1$ kJ/m^3 or 18.62 MGOe (as can be seen in Fig. 6), and its coercivity was $H_c = 4.3$ kOe [22]. Thus, it can be seen that the coercivity and M_s value were reduced by La substitution. Similar to our finding, a previous study on the Sr-hexaferrite magnets showed that the substitution of Sm along with the other rare-earth substitutions such as La, Pr, and Nd had a beneficial effect on the coercivity of Sr-hexaferrite [23]. However, in another study, Co–Mg co-doping caused a drastic decrease in the coercivity from 2.3 kOe (undoped) to 0.43 kOe (doped). This effect was attributed to the soft magnetic nature of the sample [16]. On the other hand, the reduction in the saturation magnetization M_s by the La and/or Y substitution was observed in our study (from 25.4 emu/g for single La to 9.40 emu/g for La–Y substitution). This was not the case in a previous study, in which M_s value increased by 2.6% with the Si–Li substitution [18]. The improvement of the coercivity by La substitution that was found in our study

TABLE II

Magnetization and other magnetic data.

Label	M_s [emu/g]	M_r [emu/g]	H_c [Oe]	M_r/M_s
SFL	25.4	12.8	2080	0.50
SFY	15.4	5.50	502	0.36
SFLY2	9.40	2.70	155	0.30
SFLY1	8.90	2.50	155	0.30

was not observed in another study, where the Gd and Cu substitution reduced the coercivity from 5.3 to 1.5 kOe. This result was explained by the reduction in the magnetic anisotropy due to the substitution of Gd^{3+} at the Sr^{2+} site and Cu^{2+} at the Fe^{3+} site in the hexaferrite lattice [19].

The SFL sample exhibited a $(BH)_{\max}$ value of 1.99 kJ/m^3 or 0.3 MGOe, and the value of the SFY sample was 0.2 kJ/m^3 or 0.03 MGOe. Similar max. energy product values were found in a previous study where undoped composition had a $(BH)_{\max}$ value of 0.24 MGOe [19], which was close to that of the SFY sample. In the same study, the doped composition exhibited a $(BH)_{\max}$ value of 1.33 MGOe [19], which was close to that of the SFL sample in our study.

According to Bahadur and colleagues [24], the energy product of 1.0 MGOe was obtained when the sample was sintered at 700°C. For particles of 50 nm, the saturation magnetization M_s of 33 emu/g and the coercivity H_c of 0.58 kOe were obtained, whereas the M_s and H_c values of 35 emu/g and 4.8 kOe, respectively, were obtained for the particles of 70 nm [25–27], for comparison with our results. In our study, saturation magnetization was 23% lower than these values, and there was a noticeable improvement in our coercivity value compared to the above value of 0.58 kOe.

The saturation magnetization value obtained from the co-precipitated sample, which was sintered at 640°C, was 25 emu/g [28]. According to the study of Shepherd and colleagues [29], the coercivity value H_c of the hexaferrite sample was determined to be 5.26 kOe. Another study on the M-type hexaferrite found a coercivity value of 5 kOe for a Fe:Ba ratio of 1:1 after the sintering process at 700°C [24]. The saturation magnetization in our study was 1.6% higher than those given in the above studies, whereas our coercivity value was lower than the values given in those studies.

The squareness ratio (M_r/M_s) of the sample SFL, which showed the highest value, was determined to be 0.50, and this value was close to that measured in the reference material of pure strontium hexaferrite (0.62) [22]. Rambabu and co-workers [20] (2024) found a M_r/M_s value of 0.49 for their La-substituted hexaferrite sample. In Gd–Cu-doped hexaferrite nanoparticles, the measured M_r/M_s value was 0.511 [19], which is very close to that obtained in our study. This value

reflects the ability of the sample to retain the magnetization under the magnetic field application, and the value obtained for the SFL sample showed that this sample is suitable in terms of strong magnetization and the stability of the magnetization [30]. Since the squareness ratio (M_r/M_s) in our study is larger than 0.5, it can be said that the change in the magnetization can be realized by the rotation [19]. This property is desired for the permanent magnets. Therefore, it is reasonable to suggest that the incorporation of the new rare-earth cations into the hexaferrite lattice could be important for improving the ferrimagnetic properties of strontium hexaferrite materials.

4. Conclusions

This study reports the production process of $SrFe_{12}O_{19}$ materials successfully by the solid-state reaction at 1250°C for 3 h. The properties of the synthesized samples were discussed in terms of binary La–Y and Co doping. Depending on the magnetic results, it was determined that doping with La at $x = 0.2$ yields the best results. The values of the saturation M_s and remanence M_r magnetization of the SFL sample were determined to be 25.4 and 12.8 emu/g, respectively. The coercivity value H_c was 2.08 kOe.

These highest magnetization values observed in this sample can be attributed to the amount of the main phase Sr-hexaferrite. The maximum energy product $(BH)_{\max}$ values were estimated by taking the product of the coercivity field and the remanence magnetization. These values are considered to be comparative indications of hysteresis areas of the samples.

The study also revealed that the main phase in all of the samples was $SrFe_{12}O_{19}$, and the diffraction peaks showed that the formation of $SrFe_{12}O_{19}$ compound was accomplished completely without any impurity phases. XRD patterns indicated that the binary La–Y and Co doping affected both the peak intensities and the positions of the Bragg angles. Based on the structural and ferrimagnetic results, it can be suggested that new rare-earth cations could be incorporated into the hexagonal lattice to improve the magnetic properties of the strontium hexaferrites.

Acknowledgments

The author would like to acknowledge Dokuz Eylül University, Izmir, for providing the XRD analysis and Electronic Materials Production Laboratory (EMUM) for VSM measurements. The author would also like to acknowledge Nilüfer Tuba Yılmaz and Murat Palut for sintering equipment support.

References

[1] A. Radon, A. Wlodarczyk, L. Sieron et al., *Sci. Rep.* **13**, 7860 (2023).

[2] A. Ur Rashid, P. Southern, J.A. Darr, S. Awan, S. Manzoor, *J. Magn. Magn. Mater.* **344**, 134 (2013).

[3] A. Lewinska, A. Radon, K. Gil et al., *ACS Appl. Mater. Interfaces* **16**, 15457 (2024).

[4] A. Radon, M.K.-Gawel, D. Lukowiec, P. Gebara, K.C.-Andraczke, A.K.-Burian, P. Wlodarczyk, M. Polak, R. Babilas, *Materials* **14**, 5241 (2021).

[5] A. Radon, J. Kubacki, M.K.-Gawel, P. Gebara, L. Hawelek, S. Topolska, D. Lukowiec, *J. Phys. Chem. Solids* **145**, 109530 (2020).

[6] J.R. Martinelli, F.F. Sene, C.N. Kamikawachi, C.S. de M. Partiti, D.R. Cornejo, *J. Non-Cryst. Solids* **356**, 2683 (2010).

[7] J. Wang, Y. Wu, Y. Zhu, P. Wang, *Mater. Lett.* **61**, 1522 (2007).

[8] Y. Li, Q. Wang, H. Yang, *Curr. Appl. Phys.* **9**, 1375 (2009).

[9] H. Sözeri, *J. Magn. Magn. Mater.* **321**, 2717 (2009).

[10] A. Radon, A. Ciuraszkiewicz, L. Hawelek, J. Kubacki, M.K. Gawel, D. Lukowiec, P. Gebara, A.K. Sobczak, A.K. Burian, *Scr. Mater.* **244**, 116020 (2024).

[11] J.M. Radwon, M.M. Rashad, M.M. Hessien, *J. Alloys Compd.* **453**, 304 (2008).

[12] K.S. Martirosyan, E. Galstyan, S.M. Hossain, Yi-Ju Wang, D. Litnivov, *Mater. Sci. Eng. B* **176**, 8 (2011).

[13] H.P. Steier, J. Requena, J.S. Moya, *J. Mater. Res.* **14**, 3647 (1999).

[14] R.C. Ropp in: *Solid State Chemistry*, Elsevier Science, Amsterdam 2003, p. 129.

[15] J. Huang, H. Zhuang, W. Lan Li, *Mater. Res. Bull.* **38**, 149 (2003).

[16] G. Sriramulu, K. Praveena, B. Ravinder Reddy, A. Kandasami, S. Katlakunta, *J. Magn. Magn. Mater.* **583**, 171046 (2023).

[17] A. Alipour, Sh. Torkian, A. Ghasemi, M. Tavoosi, G.R. Gordani, *Ceram. Int.* **47**, 2463 (2021).

[18] J.-Y. You, K. Lee, Y.-M. Kang, S.-I. Yoo, *Appl. Sci.* **12**, 12295 (2022).

[19] R. Islam, M.K.R. Khan, S. Hossain, M.M. Rahman, M.M. Haque, M. Aliuzzaman, M.K. Alam, M.S.I. Sarker, *RSC Adv.* **14**, 7314 (2024).

[20] Ch. Rambabu, S.K. Subrahmanya, Ch. Shivanarayana et al., *Inorg. Chem. Commun.* **134**, 109053 (2021).

[21] Comenius University, Bratislava Faculty of Pharmacy, Physics lecture: "Density Determination by Pycnometer", access through www.fpharm.uniba.sk.

[22] B. Ertug, "Synthesis and Characterization of Cu–Co Substituted Strontium Hexaferrite for Magnetic Applications", *Mater. Sci.* (2024) (in press).

[23] J.F. Wang, C.B. Ponton, I.R. Harris, *J. Magn. Magn. Mater.* **298**, 122 (2006).

[24] D. Bahadur, S. Rajakumar, A. Kumar, *J. Chem. Sci.* **118**, 15 (2006).

[25] V. Sankaranarayanan, Q. Pankhurst, D. Dickson, C. Johnson, *J. Magn. Magn. Mater.* **120**, 73 (1993).

[26] V. Sankaranarayanan, D. Khan, *J. Magn. Magn. Mater.* **153**, 337 (1996).

[27] V. Sankaranarayanan, Q. Pankhurst, D. Dickson, C. Johnson, *J. Magn. Magn. Mater.* **125**, 199 (1993).

[28] J. Matutes-Aquino, S. Diaz-Castanon, M. Mirabal-Garcia, S. Palomares-Sanchez, *Scr. Mater.* **42**, 295 (2000).

[29] P. Shepherd, K.K. Mallick, R.J. Green, *J. Magn. Magn. Mater.* **311**, 683 (2007).

[30] The Squareness of the Magnetic Properties, 2013.